Inorganic Materials, Vol. 39, No. 7, 2003, pp. 701–709. Translated from Neorganicheskie Materialy, Vol. 39, No. 7, 2003, pp. 827–836.

$(Mo,W)_5Si_3$–$(Mo,W)Si_2$ Eutectics: Properties and Application in Composite Materials

B. A. Gnesin, P. A. Gurzhiyants, and E. B. Borisenko

Institute of Solid State Physics, Russian Academy of Sciences, Chernogolovka, Moscow oblast, 142432 Russia

e-mail: gnesin@issp.ac.ru

Received August 6, 2002; in final form, December 18, 2002

Abstract—Experimental data are presented on $(Mo,W)_5Si_3$ and $(Mo,W)Si_2$ solid solutions and are analyzed using the known phase diagrams of the binary systems Mo–Si and W–Si. It is shown that, with increasing tungsten content, the melting temperature of the $(Mo,W)_5Si_3$–$(Mo,W)Si_2$ eutectic rises. Surprisingly, the alloys with W : Mo atomic ratios close to unity are found to contain, along with the silicide solid solutions, molybdenum disilicide almost free of tungsten. The mean room-temperature hardness of the eutectic alloys varies nonmonotonically with tungsten content and shows maxima at ≃33 and ≃75 at. % W. The surface texture is found to have a significant effect on the rate of high-temperature gas corrosion. The possibility of compositional control (variations in the W : Mo and $(Mo,W)_5Si_3$: $(Mo,W)Si_2$ ratios) over the thermal expansion of the alloys is analyzed. Data are presented on the temperature-dependent resistivity of SiC-matrix composites.

INTRODUCTION

The Mo_5Si_3–$MoSi_2$ and W_5Si_3–WSi_2 eutectics [1], as well as the series of $(Mo,W)_5Si_3$–$(Mo,W)Si_2$ mixed eutectics, are of great interest for many technological applications requiring high-temperature materials. They can be used as matrices for high-temperature, heat-resistant materials reinforced with silicon carbide or carbon materials (graphite layers, carbon fibers, and others [2–4]), in producing heat-resistant coatings on carbon and silicon carbide materials and refractory metals and alloys, and in joining any combinations of carbon and silicon carbide materials and refractory metals [5]. The properties of the mixed eutectics, such as the thermal expansion coefficient, mechanical strength, and thermal-shock resistance, can be tuned by varying the relative amounts of molybdenum and tungsten.

A literature search revealed no phase-diagram data for the ternary system Mo–W–Si in the region between the Mo_5Si_3–W_5Si_3 and $MoSi_2$–WSi_2 joins. The phase relations in this region can be tentatively inferred from the available data. According to the data presented in [6], the Mo_5Si_3–W_5Si_3 and $MoSi_2$–WSi_2 joins are pseudobinary and contain continuous series of $(Mo,W)_5Si_3$ and $(Mo,W)Si_2$ solid solutions. Therefore, there is no ternary eutectic, and the crystallization of $(Mo,W)_5Si_3$–$(Mo,W)Si_2$ eutectics terminates with liquid compositions near the line of binary eutectics (eutectic thalweg) (Fig. 1), which connects the W_5Si_3–WSi_2 and Mo_5Si_3–$MoSi_2$ eutectics. With increasing molybdenum content, the eutectic temperature decreases, since the melting point of the W_5Si_3–WSi_2 eutectic is 2013°C, and that of the Mo_5Si_3–$MoSi_2$ eutectic is 1900°C [1]. However, no solid experimental evidence has been reported to date for the existence of continuous series of $(Mo,W)_5Si_3$ and $(Mo,W)Si_2$ solid solutions.

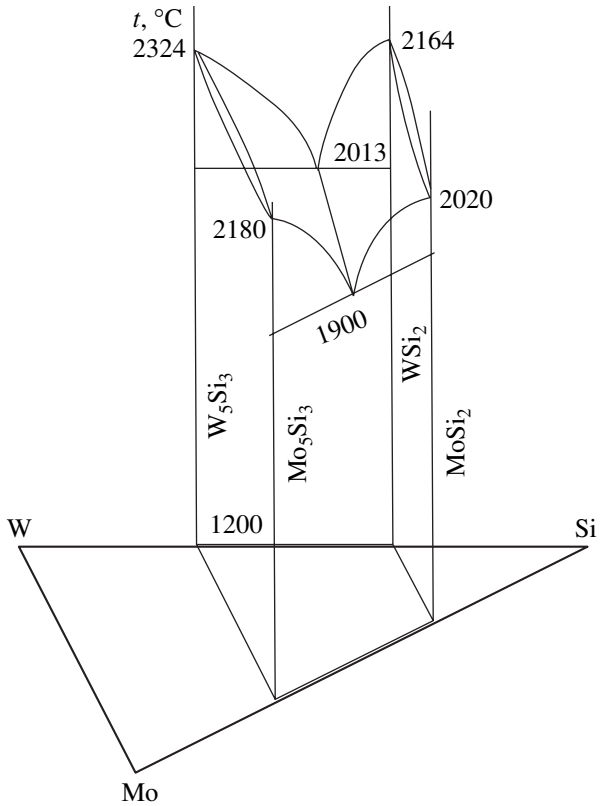

Fig. 1. Assumed liquidus relations in the Mo–W–Si system between the Mo_5Si_3–W_5Si_3 and $MoSi_2$–WSi_2 joins.

0020-1685/03/3907-0701$25.00

Molybdenum silicides have a wider variety of different crystal structures compared to tungsten silicides. In the composition range of interest here, there are only two tungsten silicides: WSi_2 (JCPDS Powder Diffraction Data File, 11-195), which has a tetragonal structure (sp. gr. *I*4/*mmm*, $MoSi_2$ type) with lattice parameters $a = 3.211$ Å and $c = 7.829$ Å, and W_5Si_3 (16-261), which also has a tetragonal structure (*I*4/*mcm*, W_5Si_3 type, $a = 9.601$ Å, $c = 4.972$ Å). The corresponding molybdenum silicides have the same structures and are very close in lattice parameters to the tungsten analogs: $MoSi_2$ (41-612, *I*4/*mmm*, $a = 3.2047$ Å, $c = 7.8450$ Å) and Mo_5Si_3 (34-371, *I*4/*mcm*, $a = 9.6483$ Å, $c = 4.9135$ Å). It is, therefore, reasonable to expect that the isomorphous molybdenum and tungsten silicides form continuous series of solid solutions [6], but could not find reports on experimental studies addressing this issue.

In addition to the tetragonal silicides Mo_5Si_3 and $MoSi_2$, the Mo–Si system contains hexagonal $MoSi_2$ (17-917, sp. gr. $P6_222$), which forms from tetragonal $MoSi_2$ as a result of a phase transition above 1900°C [1]. The W–Si system contains no hexagonal silicides. Hexagonal $MoSi_2$ may form well below 1900°C, e.g., at 700–800°C (17-917).

There is also information about another tetragonal phase of Mo_5Si_3 (17-415), which belongs to the same space group (*I*4/*mcm*) as the aforementioned phase Mo_5Si_3 (34-371). These phases are close in *d* spacings, but the x-ray diffraction (XRD) pattern of the latter contains a larger number of lines. The difference in *d* spacings does not exceed 0.016 Å, and the additional peaks from the phase described in (34-371) are rather weak (<10%). The XRD pattern of yet another molybdenum silicide $MoSi_{0.65}$ (15-94) contains only one additional line in comparison with the phase described in (34-371): $d = 2.57$ Å ($I = 30\%$). For the other lines, the difference in *d* spacings is within 0.017 Å. Since the $MoSi_{0.65}$ stoichiometry ($Mo_5Si_{3.25}$) is close to Mo_5Si_3, it is reasonable to assume that the difference in XRD data is related to the difference in preparation conditions. The increased Si content may correspond to the Si-rich phase boundary of Mo_5Si_3 (according to the Mo–Si phase diagram, the width of the homogeneity range of Mo_5Si_3 is 3 at. %). The line with $d \simeq 2.57$ Å may be due to hexagonal $MoSi_2$ (17-917), which has $d_{102} = 2.53$ Å ($I = 25\%$). Moreover, the material in question might contain impurity phases, e.g., some polytypes of silicon carbide (which have *d* spacings close to 2.57 Å) or a Nowotny phase ($d = 2.52$ Å). Thus, the origin of $MoSi_{0.65}$ is not yet fully understood, and this phase, though described in the JCPDS PDF, will be left out of consideration here. Note also that, in the composition range of interest, the only phases in the commonly accepted Mo–Si phase diagram are $MoSi_2$ and Mo_5Si_3. As will be shown below, these phases can be identified with certainty by microanalysis and XRD.

Note also the hexagonal Nowotny phase (43-1199, sp. gr. $P6_222$, $a = 7.29260$ Å, $c = 5.0439$ Å) with the recommended formula $Mo_{4.8}Si_3C_{0.6}$. Although this phase contains an appreciable amount of carbon, our experimental results demonstrate that it can be obtained even from carbon-free starting mixtures, as a result of melt contamination (carbon parts of the furnace or graphite crucible). No W analog of the Nowotny phase is represented in the JCPDS PDF. Such a phase was mentioned in early reports, but its existence was not confirmed in later studies [7].

The existence of hexagonal $MoSi_2$ and the formation of Nowotny phases as a result of carbon dissolution in $MoSi_2$ and Mo_5Si_3 may impede the formation of solid solutions between molybdenum and tungsten silicides.

Note that, in studies of the Mo–W–C system, Rudy *et al.* [8] identified (Mo,W)C and $(Mo,W)_2C$ solid solutions, even though there is no carbide of composition MoC. Thus, the solid-solution ranges of $(Mo,W)_5Si_3$ and $(Mo,W)Si_2$ must be assessed by direct experimental techniques.

In this paper, we report the phase composition, structure, and properties of silicide phases with compositions along the straight line connecting the Mo_5Si_3–$MoSi_2$ and W_5Si_3–WSi_2 eutectics, which approximates the eutectic line in the ternary system. The exact position of the eutectic line was not located.

EXPERIMENTAL

Samples for this investigation were prepared in a high-temperature (≤2300°C) resistance-heated graphite furnace under a pure argon atmosphere. As starting materials, we used MCh molybdenum, VCh tungsten, and semiconductor-grade silicon powders. The samples (7–15 g) were melted in siliconized graphite crucibles. Most of the samples were melted twice. After complete melting, the holding time was no longer than 2 min to avoid contamination. The melt was homogenized owing to convection and by vibration stirring at a frequency of 3–15 Hz with an amplitude of 0.1–0.8 mm. The melting point was determined by a Promin' brightness-temperature pyrometer. The calibration of the pyrometer was checked by melting reference substances in the same furnace. Repeated measurements on the references and samples showed that the deviation from the true temperature of complete melting (liquidus temperature) was typically no greater than 10–20°C.

Specimens for microstructural examination were prepared by grinding and polishing with diamond powders and pastes. The polishing sequence included 60/40 to 0.5/0 μm steps. No chemical or electrochemical polishing was performed.

XRD studies were carried out on a DRON-3.0 diffractometer (upgraded at the Institute of Solid State

Physics, Russian Academy of Sciences) with monochromatized MoK_α radiation, which ensured a larger penetration depth (from 2 to 12 μm, depending on the silicide composition and experimental geometry) compared to CuK_α radiation. XRD patterns were recorded in the range $2\theta = 10°$–$28°$ (d = 1.58–4.07 Å). The x-ray beam was collimated using a 0.25-mm receiving slit and 2.5° Soller slits in both the incident and diffracted beams.

In texture analysis by the tilting method (in Schultz reflection geometry) [9], we used a Euler cradle unit. Pole figures were obtained at tilt angles (polar angles) $\vartheta = 0°$–$70°$ and azimuth angles $\varphi = 0°$–$360°$ (both at 5° intervals). Initially, the sample was mounted at $\vartheta = 70°$ and $\varphi = 0°$. The pulses passed by the amplitude analyzer were counted for 3 s, and the result was stored, together with the ϑ and φ values. Then, φ was changed by an increment of 5° and the counting cycle was repeated. After φ attained 360°, ϑ was reduced by 5° and the next φ scan was carried out. Such cycles were repeated until $\vartheta = 0°$. The intensity data were corrected for the defocusing and background. No absorption correction was applied because the sample was sufficiently thick [9]. The diameter of the samples for texture analysis was 18–25 mm.

Microstructures were examined under a Neophot-32 optical microscope. The best contrast was achieved in polarized light, by adjusting the angle between the entrance and exit polarizers. Secondary electron (SE) and backscattered electron (BSE) images and x-ray maps were obtained on DSM-960 and JSM-25S scanning electron microscopes (SEM).

X-ray microanalysis was carried out with a CAMEBAX instrument (Institute of Experimental Mineralogy, Russian Academy of Sciences) operated at 15 kV (Si detector, beam diameter of 5–10 μm, counting time of 70 s, amplitude distribution analysis). The composition of major phases was determined by taking averages over at least five repeated measurements. As analytical standards, we used dense molybdenum, tungsten, and silicon samples close in purity to the starting materials. The uncertainty in concentrations was typically no higher than 1–2 at. %, as determined in reproducibility tests on samples and standards.

Microhardness was determined with a PMT-3 tester from the geometric mean of the two indent diagonals. The indent separation was at least three times as large as the indent diagonal. Indents were made at a load of 1 N. The calibration of the tester was checked using certified microhardness standards.

Electrical resistivity was determined in a four-point configuration, using digital voltmeters to measure the voltage drop across a current-measuring shunt (75 mV/200 A) placed in series and the water-cooled Cu current leads. The samples were heated resistively in air. The sample temperature was measured by a Promin' brightness-temperature pyrometer.

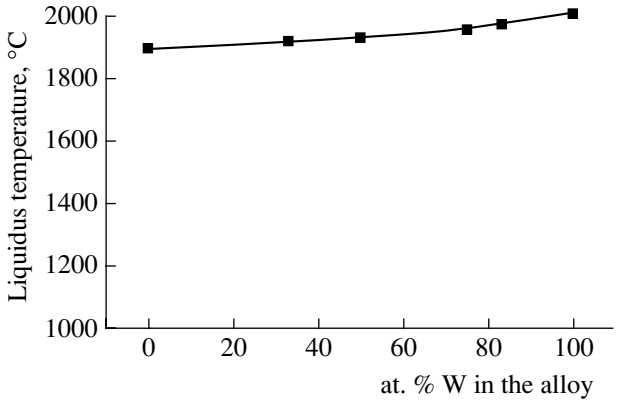

Fig. 2. Liquidus temperature as a function of tungsten content for compositions along the straight line connecting the Mo_5Si_3–$MoSi_2$ and W_5Si_3–WSi_2 eutectics.

RESULTS AND DISCUSSION

Liquidus temperature near the eutectic line. As pointed out above, the liquidus temperature was measured for compositions along the straight line connecting the Mo_5Si_3–$MoSi_2$ and W_5Si_3–WSi_2 eutectics, rather than along the line of binary silicide eutectics. The temperature in the furnace was raised slowly at a constant heater power. The melting range was relatively narrow, 10 to 30°C. Attempts to measure the solidification temperature were unsuccessful: the crystallization time was too short (2–10 s) to determine the crystallization onset temperature. The data in Fig. 2 demonstrate that, with increasing tungsten content, the liquidus temperature rises steadily. The slope is steeper at tungsten contents above 50 at. %. The melting points of the Mo_5Si_3–$MoSi_2$ and W_5Si_3–WSi_2 eutectics coincide to within 5°C with those reported in [1].

Thus, our results confirm that the liquidus temperature rises monotonically with tungsten content for the compositions under consideration.

Structure and composition of the samples. For most of the samples, the melt was heated to 2100°C before crystallization. In addition, the melt with Mo : W = 1 was solidified after heating to 1950°C (the liquidus temperature of this composition was determined to be 1930 ± 15°C). The melt was heated to well above the liquidus temperature because such overheatings are common in practice. Moreover, heating to 100–150°C above the liquidus temperature ensures, as a rule, melt homogenization.

Polished sections for microstructural analysis were prepared parallel to the crucible bottom. The sample with Mo : W = 1 was found to have the least pronounced texture. Some of the grains in that sample were more than 20 μm across. The BSE image of

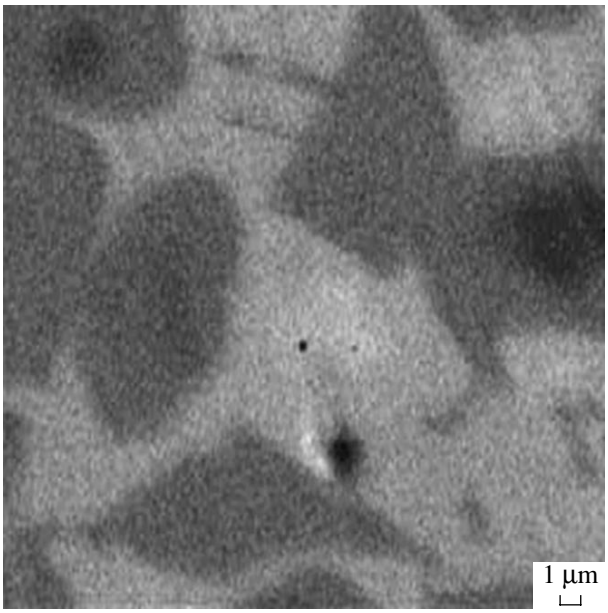

Fig. 3. BSE image of the sample with Mo : W = 1. $(Mo,W)Si_2$ and $(Mo,W)_5Si_3$ grains are seen as dark and light areas, respectively. The darkest area within the large $(Mo,W)Si_2$ grain is highly deficient in tungsten.

$(Mo,W)Si_2$ with Mo : W = 1 showed dark inclusions (Fig. 3). The beam was focused to the pore seen below the center of the image.

The composition of the dark inclusions is close to $MoSi_2$; that is, they are highly deficient in tungsten compared to $Mo_{0.5}W_{0.5}Si_2$ (Table 1). For this reason, in Table 1 we indicate two compositions of disilicides in the sample with Mo : W = 1, one close to the equiatomic composition, and the other highly deficient in tungsten.

Table 1. Compositions of $(Mo,W)_5Si_3$ and $(Mo,W)Si_2$ as functions of the tungsten content

at. % W	Melt temperature before crystallization, °C	at. % W in $(Mo,W)Si_2$	at. % W in $(Mo,W)_5Si_3$
0	2100	0	0
33	2100	26.9 ± 0.8	35.1 ± 4.7
50	2100	45.8 ± 9.8	63.1 ± 9.1
		1.6 ± 2.5*	
50	1950	46.1 ± 1.3	57.5 ± 5.2
		13.7 ± 19.2*	
75	2100	72.7 ± 0.6	81.7 ± 2.7
83	2100	81.6 ± 1.1	87.7 ± 0.6
100	2100	100	100

Note: Average values (at. %) and standard deviations for compositions along the straight line shown in Fig. 1.

* Dark inclusions.

The sample obtained after heating to 1950°C was also found to contain disilicide inclusions highly deficient in tungsten, but the tungsten content of those inclusions was notably higher than that after heating to 2100°C (Table 1). In both samples, the amount of the tungsten-deficient disilicide (well observed on the background of the disilicide with a nearly nominal tungsten content) does not exceed 10–20 vol %.

In the other samples, no significant variations in the compositions of $(Mo,W)_5Si_3$ and $(Mo,W)Si_2$ were detected, in agreement with x-ray microanalysis results (Table 1). The silicon content of $(Mo,W)_5Si_3$ was 38.00–42.50 at. % (the stoichiometric value is 37.5 at. %). At the same time, in Mo-enriched silicides of this type, the silicon content is increased by about 1.5 at. %, which corresponds to the composition region of Mo_5Si_3 in the Mo–Si phase diagram [1]. In this study, the highest silicon content of Mo_5Si_3 was indeed observed in the most Mo-rich samples. The silicon content of the disilicide phases was 65.45–68.44 at. % (the stoichiometric value is 66.67 at. %.

It follows from our data that the compositions of phases scatter most widely at Mo : W = 1. For $(Mo,W)Si_2$ and $(Mo,W)_5Si_3$, the scatter can be reduced markedly by lowering the melt overheating temperature, but it remains rather large in the tungsten-deficient disilicide. We could not ascertain whether the presence of two disilicides in the samples with Mo : W = 1 was due to binodal decomposition, solid-state phase segregation, or inherent features of their crystallization behavior. It may also be associated with the fact that, in the ternary phase diagram, the largest deviation of the straight line connecting the W_5Si_3–WSi_2 and Mo_5Si_3–$MoSi_2$ eutectics from the true line of binary eutectics must occur at Mo : W = 1. None of these mechanisms explain why the disilicide separation occurs only at Mo : W = 1. The separation took place after heating the melt to both 1950 and 2100°C. After the smaller overheating, the composition of the tungsten-deficient disilicide was closer to the nominal composition.

In all the samples (Table 1, Fig. 4), the higher melting silicide $(Mo,W)_5Si_3$ was enriched in tungsten, the higher melting component, which raises the melting point of silicides, while the disilicide phase was enriched in molybdenum. For compositions farther away from Mo : W = 1, the deviations of the average compositions of phases from the additivity rule are smaller. No less important aspect of our results is the experimental evidence for the formation of continuous series of $(Mo,W)_5Si_3$ and $(Mo,W)Si_2$ solid solutions, which validates the assumptions made in constructing the portion of the ternary phase diagram shown in Fig. 1.

Phase composition and lattice parameters of melted samples. The phases present in the silicide alloys under consideration are rather difficult to identify by XRD, especially in the case of Mo-enriched silicides, which have a wider variety of different crystal structures compared to tungsten silicides. Carbon contamination (from the gas phase or crucible) of Mo-rich samples may also add complexity, leading to the formation of the Nowotny phase. Moreover, it cannot be ruled out that the cooling rate after melt solidification may also influence the XRD patterns of the alloys. As a result, the observed diffraction peaks often cannot be assigned to one or another phase (Fig. 5). In this respect, SEM is more informative since it easily distinguishes $(Mo,W)_5Si_3$ and $(Mo,W)Si_2$.

Table 2 presents XRD data for samples that were characterized by x-ray microanalysis. Only those four peaks are included which are easy to index, lie in the angular range where peaks from silicon carbide are missing, and can be used to determine the lattice parameters of tetragonal $(Mo,W)_5Si_3$ and $(Mo,W)Si_2$.

All of the silicide phases were found to be highly textured, irrespective of crystallization conditions. The alloys may contain hexagonal disilicides isostructural with hexagonal $MoSi_2$. The peaks from hexagonal disilicides are well observed at W contents of 33 and 50 at. % (Table 2, Fig. 5). Detailed experimental data confirming the presence of hexagonal disilicides in other samples will be presented in a forthcoming paper. The W content of the hexagonal disilicide remains unclear, especially for the Mo : W = 1 composition in the straight line connecting the Mo_5Si_3–$MoSi_2$ and W_5Si_3–WSi_2 eutectics. Only at this composition do we observe solid-state phase segregation, and it cannot be ruled out that the tungsten-deficient disilicide has a hexagonal structure.

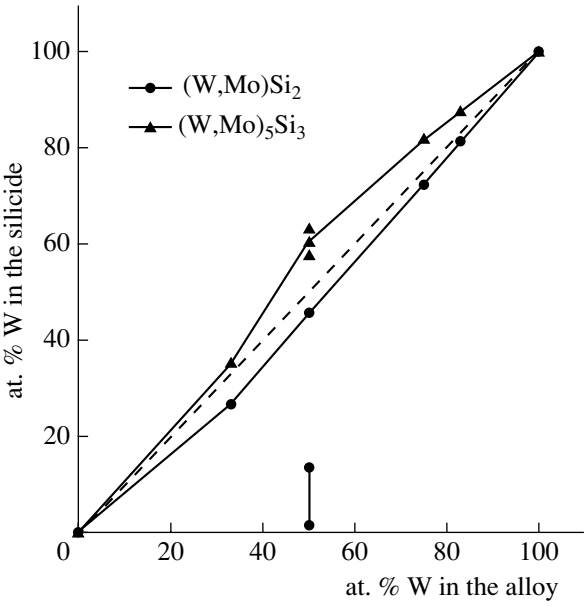

Fig. 4. W content of $(Mo,W)_5Si_3$ and $(Mo,W)Si_2$ as a function of the W content of the alloy; the dashed line corresponds to nominal compositions.

Table 2. Parameters of four diffraction peaks from silicides as functions of tungsten content in the alloys

at. % W	θ, deg	*d*, Å	*I*, arb. units	θ, deg	*d*, Å	*I*, arb. units	θ, deg	*d*, Å	*I*, arb. units	θ, deg	*d*, Å	*I*, arb. units
	3.91–3.98 Å			3.039–3.052 Å			2.976–2.97 Å			2.457–2.487 Å		
33	10.19	3.993*	5595	13.43	3.032	58	13.71	2.971	2513	16.53	2.467	48
	10.43	3.901	1501									
50 (2100°C)	10.31	3.947	241	13.36	3.049	64	13.60	2.995	199	16.35	2.494	69
							13.96	2.918	85			
50 (1950°C)	10.27	3.962*	65	13.25	3.074	262	13.90	2.931	162	16.45	2.479	98
75	10.41	3.909	86	13.31	3.060	601	13.67	2.980	388	16.51	2.470	55
83	10.43	3.902	5297	13.33	3.055	68	13.53	3.011	104	–	–	–
100	10.41	3.909	15589	–	–	–	13.65	2.984	136	–	–	–
JCPDS data	Tetragonal {002}: $MoSi_2$–3.92 Å; 31% WSi_2–3.91 Å; 50% Hexagonal {100} $MoSi_2$–3.98 Å; 10%			Tetragonal {310}: Mo_5Si_3–3.052 Å; 21% W_5Si_3–3.039 Å; 50%			Tetragonal {101}: $MoSi_2$–2.967 Å; 60% WSi_2–2.97 Å; 100%			Tetragonal {002}: Mo_5Si_3–2.457 Å; 25% W_5Si_3–2.487 Å; 30%		

* Peaks from the hexagonal disilicide.

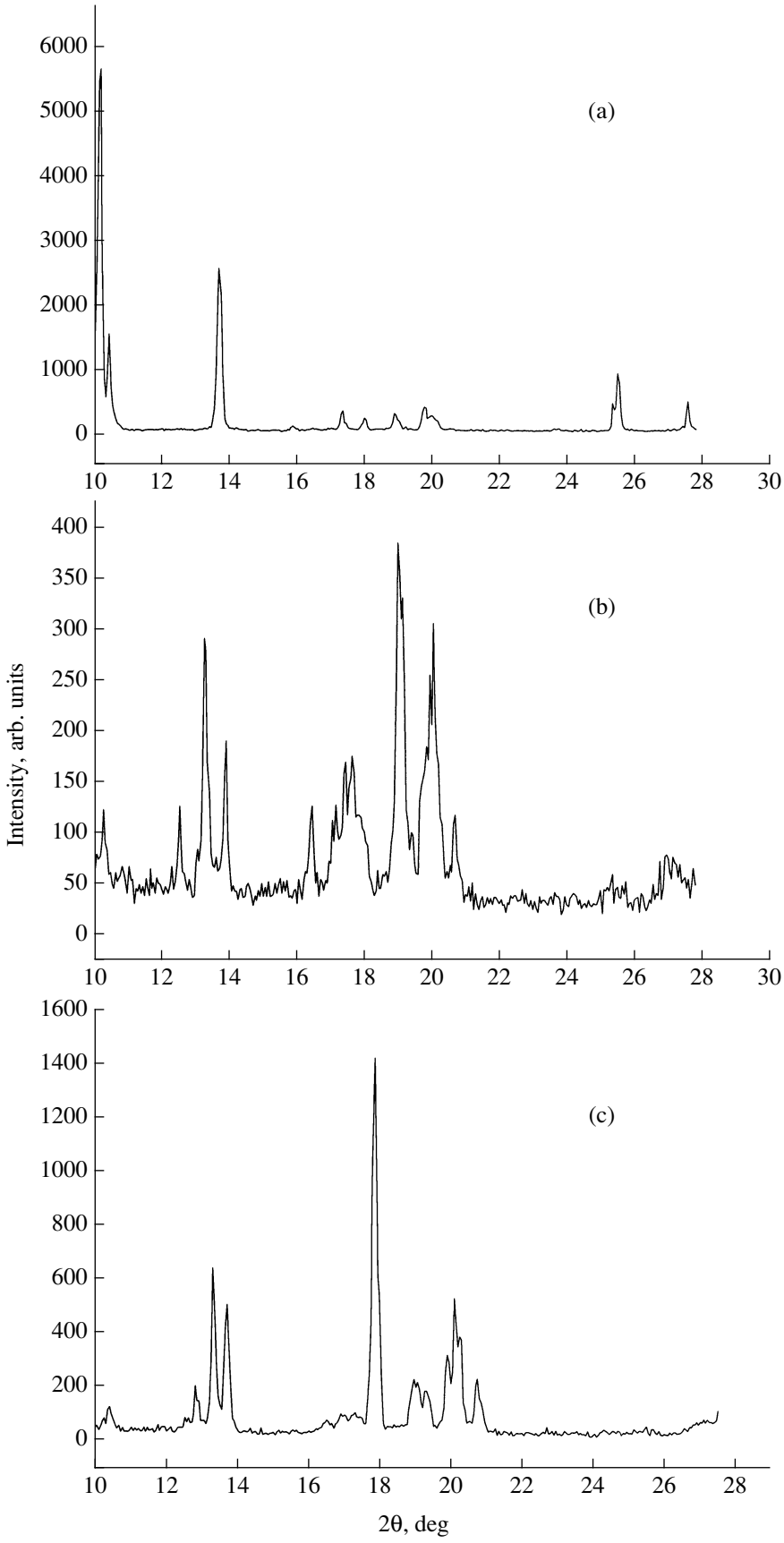

Fig. 5. XRD patterns of silicide alloys containing (a) 33, (b) 50, and (c) 75 at. % W.

The lattice parameters of tetragonal $(Mo,W)_5Si_3$ and $(Mo,W)Si_2$ vary nonmonotonically with Mo : W ratio, in contrast to what would be expected in the case of isomorphous substitution. This is clearly demonstrated by the nonmonotonic shift of all the observed reflections with increasing tungsten content (Table 2). Linear equations for lattice parameters (Å) as functions of x = Mo/(Mo + W) have the following form: $a = 9.601 + 0.019x$, $c = 4.972 - 0.085x$ for tetragonal $(Mo,W)_5Si_3$ and $a = 3.211 - 0.006x$, $c = 7.829 + 0.016x$ for tetragonal $(Mo,W)Si_2$. The observed relative intensities differ markedly from those given in the JCPDS PDF, pointing to a strong texture, especially for $2\theta < 14°$ (Fig. 5).

Microhardness. Figure 6 shows microhardness distributions in the form of ranged (ordered by the microhardness value) samples of 15–25 measurements for the alloys that were characterized by microanalysis and XRD. The relative error in microhardness measurements was typically at a level of 2% and did not exceed 4%.

The microhardness distributions displayed in Fig. 6 were constructed using the Microsoft Excel pack. The distributions adequately describe the microhardness data, duplicating many features of the parent microhardness distribution. This way of representing experimental data is more informative than the commonly used average and variance and makes it possible to reveal bimodality or asymmetry and to find the spread of the distribution for a given sample and the maximum and minimum microhardness values.

Microhardness data for $MoSi_2$, WSi_2, Mo_5Si_3, and W_5Si_3 were reported earlier in [10, 11]. The data for the disilicides scatter more widely, e.g., 600–900 GPa for $MoSi_2$. We suppose that this large scatter, markedly exceeding experimental error, may be due in some measure to anisotropy. The phases in question have tetragonal and hexagonal structures. It is well known that even diamond, a material with cubic symmetry, has a considerable anisotropy, on the order of 10%, in its hardness. Moreover, the hardness depends not only on the crystallographic orientation of the indented surface but also on the direction of the indent diagonal.

The subject of this study is the $(Mo,W)Si_2$ + $(Mo,W)_5Si_3$ eutectic. According to the data for pure molybdenum and tungsten silicides [11], the microhardness of Mo_5Si_3 must be higher. Therefore, the scatter in microhardness data is undoubtedly due to the presence of at least two different silicides. As pointed out above, some of the samples may also contain the hexagonal disilicide. The largest scatter in microhardness data was found at Mo : W = 1 (Fig. 6, curve *2*). The distribution for this sample includes at least three plateaus and seems, therefore, to be trimodal, which is probably associated with the observed disilicide separation. Our microhardness data for the W_5Si_3–WSi_2 eutectic agree well with earlier results.

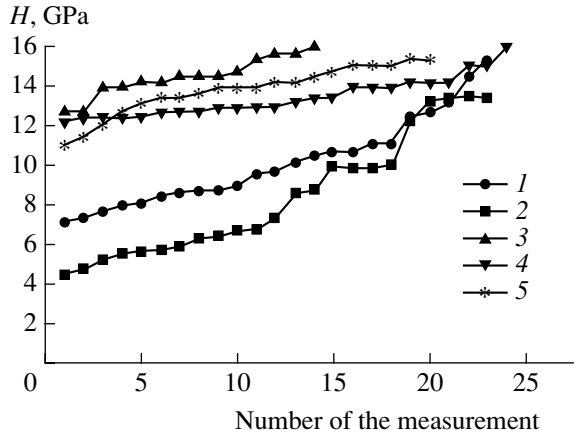

Fig. 6. Ranged microhardness distributions for near-eutectic silicide alloys containing (*1*) 100, (*2*) 50, (*3*) 83, (*4*) 25, and (*5*) 75 at. % W (the number of the measurement corresponds to the number in the ranged sample).

An important point that, for a number of compositions (33, 75, and 83 at. % W), both the mean and minimum microhardness values notably exceed these for the Mo_5Si_3–$MoSi_2$ and W_5Si_3–WSi_2 eutectics. At Mo : W = 1, there is a dip in both the mean and minimum microhardness values, just as in the Mo–W system, but the maximum value depends little on the Mo : W ratio.

Potential applications. In the past decade, there has been intense interest in refractory-metal silicides as components of high-temperature composites capable of withstanding exposure to oxidizing atmospheres. Silicon carbide is commonly thought of as the most promising reinforcing agent. Such composites have long been and continue to be used to advantage [2, 12–17]. Note that, above 1600°C, Mo_5Si_3 is more resistant to gas corrosion than $MoSi_2$ [7, 18, 19]. Moreover, at these high temperatures, tungsten silicides may be chemically more resistant than molybdenum silicides [7]. In light of this, it is reasonable to assume that $(Mo,W)_5Si_3$–$(Mo,W)Si_2$ eutectics are suitable materials for high-temperature antioxidizing coatings. Since, according to our experimental results, such eutectics wet carbon and silicon carbide materials and silicides, they can be used not only as binders and protective coatings for high-temperature composites but also as brazing solders. The use of the Mo_5Si_3–$MoSi_2$ eutectic for brazing refractory metals was reported by Cherniack and Elliot [19].

Varying the Mo : W ratio in $(Mo,W)_5Si_3$–$(Mo,W)Si_2$ eutectics, one can tune their thermal expansion coefficient. Although all of the silicides in question are close in thermal expansion, $(4–9) \times 10^{-6}$ K^{-1}, cooling and thermal cycling after brazing may give rise to distortions and cracking. It should be taken into account that the thermal expansion of the materials under consideration varies with temperature in a complex manner and that silicides can withstand significant plastic strain

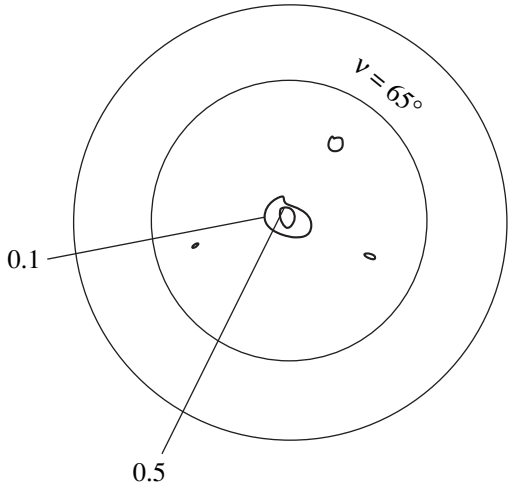

Fig. 7. {002} pole figure of tetragonal $(Mo,W)Si_2$ in a protective coating on the surface of a carbon material.

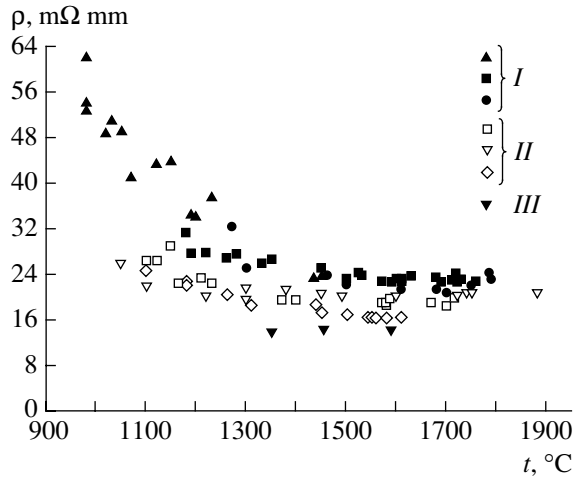

Fig. 8. Resistivity of the working region as a function of temperature at volume fractions of silicon carbide η = (*I*) 0.65, (*II*) 0.58, and (*III*) 0.52.

above 1200°C. For example, the best brazing solder for joining silicon carbide infiltrated with silicides to MPG6 graphite is the $(Mo,W)_5Si_3$–$(Mo,W)Si_2$ eutectic containing ≃25 at. % W. Increasing the $(Mo,W)_5Si_3$ content of the brazing solder (the deviation from the eutectic line) sharply reduces its thermal expansion.

The increase in the liquidus temperature with increasing tungsten content is of practical significance: protective coatings may consist of many layers, and brazing and coating steps can be performed in different sequences. The only necessary condition is that the temperature of each operation be lower than that of the preceding operation. Our experience shows that, for this purpose, the range of liquidus temperatures from 1900 to 2010°C is quite sufficient.

In contrast to conventional processes for applying protective coatings by powder-processing techniques, directional solidification of high-temperature silicide eutectics allows one to produce highly oriented coatings. The rate of high-temperature gas corrosion may depend strongly on the coating texture [5]. Figure 7 shows the {002} pole figure for tetragonal $(Mo,W)Si_2$ in a protective coating on the surface of a carbon material. The strong central peak attests to a (001) preferential alignment almost parallel to the sample surface. The intensity of the 002 reflection drops by more than a factor of 10 as the sample is tilted 15° away from (001) and by more than a factor of 20 at a 25° tilt. Measurements above 1200°C show that the preferential orientation reduces the oxidation rate (weight loss per unit time per unit surface area) by at least a factor of 5.

An important application field for composites containing refractory-metal silicide eutectics is the production of high-temperature electrical heaters. The current leads of such heaters can be made of carbon materials with reliable graphite contacts for operation at temperatures below 200°C. To the current leads, one can solder a working region of a silicon carbide composite produced by infiltrating a porous body with $(Mo,W)_5Si_3$–$(Mo,W)Si_2$ eutectics. The working region can be protected with a coating of constituent silicides textured as a result of directional solidification. The oxidation rate of such coatings is substantially lower in comparison with $MoSi_2$-based powder coatings. All of this markedly extends the ranges of possible designs and performance parameters of heaters.

One important characteristic of heaters is the temperature dependence of the electrical resistivity of the working region. Figure 8 shows data (1100–1700°C) for three sets of heaters prepared by infiltrating silicon carbide bodies with eutectic melts. The same melts were used to produce protective coatings. In our experiments, samples differing in the volume fraction of silicon carbide (η = (*I*) 0.65, (*II*) 0.58, (*III*) 0.52) were infiltrated with $(Mo,W)_5Si_3$–$(Mo,W)Si_2$ eutectics differing in tungsten content. It follows from our results that the shape of the resistivity versus temperature curve is governed by the conductivity of the silicon carbide component and depends only weakly on the eutectic composition. Reducing the volume fraction of silicon carbide in the heater material reduces its resistivity and lowers the temperature starting at which the heater resistivity rises with temperature (PTCR behavior). At a volume fraction of silicon carbide near 0.5, we obtained an extended region of PTCR behavior in the temperature range of interest.

ACKNOWLEDGMENTS

This work was supported by the Russian Foundation for Basic Research and the Moscow Oblast Government (joint grant no. 01-02-97028).

REFERENCES

1. *Binary Alloy Phase Diagrams*, Massalski, Th. B., Ed., Metals Park: American Society for Metals, 1986.
2. Gnesin, B.A., Gurzhiyants, P.A., and Epel'baum, B.M., Mo–Si–C Composite Ceramics Prepared by Directional Solidification, *Neorg. Mater.*, 1998, vol. 34, no. 2, pp. 234–240 [*Inorg. Mater.* (Engl. Transl.), vol. 34, no. 2, pp. 178–183].
3. Gnesin, B.A., Epel'baum, B.M., and Gurzhiyants, P.A., RF Patent 2154122, *Byull. Izobret.*, 2000, no. 22.
4. Gnesin, B.A. and Gurzhiyants, P.A., RF Patent 2160790, *Byull. Izobret.*, 2000, no. 35.
5. Gnesin, B.A. and Gurzhiyants, P.A., RF Patent 2178958, *Byull. Izobret.*, 2002, no. 3.
6. Zakharov, A.M., *Diagrammy sostoyanii dvoinykh i troinykh sistem* (Phase Diagrams of Binary and Ternary Systems), Moscow: Metallurgiya, 1978.
7. Samsonov, G.V., Dvorina, L.A., and Rud', B.M., *Silitsidy* (Silicides), Moscow: Metallurgiya, 1979.
8. Rudy, E., Kieffer, D.F., and Baroch, E., HfN Coatings for Cemented Carbides and New Hard-Facing Alloys on the Basis $(Mo,W)C$–$(Mo,W)_2C$, *Planseeber. Pulvermetall.*, 1978, vol. 26, no. 2, pp. 105–115.
9. Wasserman, G. and Grewen, J., *Texturen metallischer Werkstoffe*, Berlin: Springer, 1962, 2nd ed. Translated under the title *Tekstury metallicheskikh materialov*, Moscow: Metallurgiya, 1969.
10. Chu, R. and Thoma, D.J., Processing and Properties of Mo_5Si_3 Single Crystals, *Annual Conf. on Composites, Advanced Ceramics Materials, and Structures*, Cocoa Beach, 1998.
11. Andrievskii, A.R. and Spivak, I.I., *Prochnost' tugoplavkikh soedinenii i materialov na ikh osnove* (Strength of Refractory Compounds and Related Materials), Chelyabinsk: Metallurgiya, 1986.
12. Wejnarth, A.R., US Patent 2412373, 1943.
13. Schrevelius, N.G., US Patent 3036017, 1954.
14. Wejnarth, A.R., US Patent 3009886, 1958.
15. Maloney, M.J. and Hecht, R.J., Development of Continuous-Fiber-Reinforced $MoSi_2$-Base Composites, *Mater. Sci. Eng., A*, 1992, vol. 155, pp. 19–31.
16. Aikin, R.V., Jr., Strengthening of Discontinuously Reinforced $MoSi_2$ Composites at High Temperatures, *Mater. Sci. Eng., A*, 1992, vol. 155, pp. 121–133.
17. Gibala, R., Ghosh, A.K., Van Aken, D.C., *et al.*, Mechanical Behavior and Interface Design of $MoSi_2$-Based Alloys and Composites, *Mater. Sci. Eng., A*, 1992, vol. 155, pp. 147–158.
18. Kasatkin, A.V. and Matvienko, I.V., Heat Resistance of Silicide Coatings on Molybdenum and Molybdenum-Based Alloys, *Neorg. Mater.*, 1994, vol. 30, no. 7, pp. 928–931 [*Inorg. Mater.* (Engl. Transl.), vol. 30, no. 7, pp. 860–863].
19. Cherniack, G.B. and Elliot, A.G., High-Temperature Behavior of $MoSi_2$ and Mo_5Si_3, *J. Am. Ceram. Soc.*, 1965, vol. 467, no. 3, pp. 136–141.